

UC Davis

UC Davis Previously Published Works

Title

FEM Analysis of Dynamic Soil-Pile-Structure Interaction in Liquefied and Laterally Spreading Ground

Permalink

<https://escholarship.org/uc/item/1sw070c3>

Journal

Earthquake Spectra, 29(3)

ISSN

8755-2930

Authors

Chang, Dongdong
Boulanger, Ross
Brandenberg, Scott
et al.

Publication Date

2013-08-01

DOI

10.1193/1.4000156

Peer reviewed

FEM Analysis of Dynamic Soil-Pile-Structure Interaction in Liquefied and Laterally Spreading Ground

Dongdong Chang,^{a)} M.EERI, Ross Boulanger,^{b)} M.EERI, Scott Brandenburg,^{c)} M.EERI, and Bruce Kutter^{b)} M.EERI

A two-dimensional nonlinear dynamic finite element (FE) model was developed and calibrated against dynamic centrifuge tests to study the behavior of soil-pile-structure systems in liquefied and laterally spreading ground during earthquakes. The centrifuge models included a simple structure supported on pile group. The soil profiles consisted of a gently sloping clay crust over liquefiable sand over dense sand. The FE model used an effective stress pressure dependent plasticity model for liquefiable soil and a total stress pressure independent plasticity model for clay, beam column elements for piles and structure, and interface springs that couple with the soil mesh for soil-structure interaction. The FE model was evaluated against recorded data for eight cases with same set of baseline parameters. Comparisons between analyses and experiments showed that the FE model was able to approximate the soil and structural responses and reproduce the lateral loads and bending moments on the piles reasonably well.

INTRODUCTION

Dynamic soil-pile-structure interaction is an important consideration in evaluating the seismic performance of pile-supported structures in liquefied and laterally spreading ground. The complexity of soil-pile-structure interaction in the presence of liquefaction has been demonstrated through a number of case history and physical modeling studies in recent years (e.g., Boulanger and Tokimatsu 2005). A number of modeling approaches have been developed to capture key aspects of behavior, but have largely focused on static analysis methods that cannot inherently model important features of dynamic behavior such as phasing between kinematic and inertia loads, response as soil liquefaction is initiated early in shaking, and dilatancy behavior following soil liquefaction. Dynamic simulations have the

^{a)} Arup, 7670 Woodway Dr. Suite 162, Houston, TX 77063

^{b)} Department of Civil and Environmental Engineering, University of California, Davis, CA 95616

^{c)} Department of Civil and Environmental Engineering, University of California, Los Angeles, CA 90095

capability to capture these more complex features of behavior, but more comparisons of such methods with high quality test data must occur to develop confidence in such methods. Evaluations against a range of recorded response measures for the soil and structural system can assist in identifying potential limitations in the numerical models. Furthermore, extensive parameter studies are often too costly and time consuming to perform experimentally, and well calibrated numerical models provide the ability to study conditions that are not fully covered by experimental data (e.g., a broader range of input ground motions, structural configurations, and soil profiles).

This paper describes the development and calibration of two-dimensional (2-D) dynamic finite element (FE) model using data from centrifuge model tests of pile-group supported structures in soil profiles that experienced liquefaction and lateral spreading during shaking. The FE model consist a beam-column model of the superstructure and piles attached to a 2-D liquefiable soil mesh by soil springs whose properties depend on liquefaction in the adjacent soil. The centrifuge tests and FE model are described first, followed by comparisons between the computed and recorded soil and structural responses in eight earthquake events. The FE model is evaluated for its ability to capture the essential features and loading mechanism of the soil-pile-structure system, and sensitivities and limitations of the FE model are discussed.

CENTRIFUGE TESTS

Two dynamic centrifuge tests were performed that involved simple structures supported by pile groups in profiles that developed liquefaction and lateral spreading during earthquake shaking. The tests were performed on the 9-m radius centrifuge at the University of California, Davis, and are described in terms of prototype units unless otherwise indicated. The two models were similar in configurations, as summarized in Table 1 and depicted by the layout of the first model (DDC01) in Figure 1. The soil profile for both tests consisted of a nonliquefiable clay crust overlying loose sand ($D_r \approx 35\%$) overlying dense sand ($D_r \approx 80\%$) with a gently sloping (4 degree) ground surface toward an open river channel. The clay crust was reconstituted Bay Mud clay with average undrained shear strength of about 33 kPa in the first test and 22 kPa in the second test. The sand layers were uniformly-graded Nevada Sand ($C_u = 1.5$, $D_{50} = 0.15$ mm). Water was used as a pore fluid. The six-pile groups included piles of outer diameters of 1.17 m spaced at four diameters center-to-center clamped by an embedded pile cap that provided a moment-resisting connection. The structure mass was 355

tonne for both tests, corresponding to an axial load of 580 kN per pile. The structures had measured fixed-base natural periods of 0.8 s for the first and 0.3 s for the second tests.

Table 1. Soil and pile properties for the centrifuge models

Test ID	Pile Group ^a	Soil Profile	Superstructure	N ^a
DDC01	Six-pile group (2x3): pile diameter b=1.17m Cap L,W,H=14.3m, 9.2m, 2.2m	0.6m Monterey sand 3.6m clay ($s_u \approx 33\text{kPa}$) 5.4m loose sand ($D_r \approx 35\%$) dense sand ($D_r \approx 75\%$)	$T_{\text{fixed-base}} = 0.8$ s	57.2g
DDC02	Six-pile group (2x3): pile diameter b=1.17m Cap L,W,H=14.3m, 9.2m, 2.2m	0.6m Monterey sand 3.6m clay ($s_u \approx 22\text{kPa}$) 5.4m loose sand ($D_r \approx 35\%$) dense sand ($D_r \approx 80\%$)	$T_{\text{fixed-base}} = 0.3$ s	57.2g

^a N = Centrifugal acceleration

Both models were tested in a flexible shear beam container (FSB2) at a centrifuge acceleration of 57.2 g, and shaken by a series of scaled realistic earthquake recordings from Port Island (83-m depth, north-south direction) during the Kobe earthquake and from the University of California, Santa Cruz (UCSC/Lick Lab, Channel 1) during the Loma Prieta earthquake. The maximum base accelerations vary from 0.13g to 0.7g. The sequence of earthquakes for both models is given in Table 2. Complete descriptions of the centrifuge models, physical observations, and data recordings are available in data reports archived on the NEES website at UC Davis. (<http://nees.ucdavis.edu/>).

Table 2. Sequence of earthquakes for each Centrifuge model

Test	1 st Motion	2 nd Motion	3 rd Motion	4 th Motion
DDC01	Small Santa Cruz (0.13g)	Medium Santa Cruz (0.35g)	Large Santa Cruz (0.66g)	Large Kobe (0.66g)
DDC02	Small Santa Cruz (0.14g)	Medium Santa Cruz (0.34g)	Large Santa Cruz (0.73g)	Large Kobe (0.62g)

The recorded responses from these centrifuge model tests were also used in the study by Brandenberg et al. (2005, 2006, 2007), wherein load transfer mechanisms were identified using back-calculation techniques. Details on those analyses and the resulting load transfer mechanisms provided important guidance on the calibration of the dynamic FE model herein.

FINITE ELEMENT MODEL

The FE modeling was performed using the open-source software platform OpenSees (<http://opensees.berkeley.edu>) with pre- and post-processing by customized commercial software GiD. The soil and the container were modeled by 2-D continuum elements, and the structure and piles were modeled by beam-column elements attached to the soil mesh by

nonlinear soil springs. The soil springs allow relative displacements between the free-field soil mesh and the piles. Soil-pile interaction is an inherently three-dimensional problem that either requires adoption of p-y elements or use of a computationally expensive three dimensional soil continuum with small enough elements around the pile to capture the interaction behavior. The capacity of the soil springs can be controlled by the effective stress in the adjacent soil mesh so that the springs can degrade as soil liquefies. The FE meshes for DDC01 are shown in Figure 2. The soil, pile, soil spring, structure, and centrifuge container models, together with sequence of analysis steps and solution algorithms are presented below.

SOIL MODELS

The soils were modeled using four node QUADup elements that model the response of solid-fluid fully coupled material based on Biot's theory of porous media. Sand was modeled by PressureDependMultiYield (PDMY) material and clay was modeled by PressureIndependMultiYield (PIMY) material by Yang and Elgamal (2002). The materials were assigned to four node quad elements with three degrees of freedom at the four corner nodes (two DOF's for displacement and one for pore pressure). Four node quad elements are known to lock in undrained loading conditions due to incompressibility. Nine-node quad elements were introduced after the work presented in this paper was completed to help solve this problem. However, mesh locking is not anticipated to be significant for the simulations presented herein because soil deformations are dominated by a simple shear mechanism that is less prone to mesh locking. Increased damping in the Newmark integrator was used to suppress high frequency oscillations that can arise from mesh locking.

The out-of-plane thickness of the soil elements is 48 m, the same with the centrifuge models. Typically the out-of-plane thickness of the 2-D mesh would be made very large to enforce plane strain conditions. However, the out-of-plane thickness was set equal to the centrifuge model container thickness in this case to capture any pinning effects introduced by the pile group. A repeat of one of the runs with the out-of-plane thickness set to 1000m resulted in computed responses that were within 3% of the cases with the 48m thickness. Hence, we conclude that the 48m thickness provided essentially plane-strain conditions and a "free-field" soil site response. In fact, an alternative approach would be to conduct the site response analysis first, without any structural elements, and subsequently input the results into the free ends of the p-y elements. However, in this case the structural mesh was included

simultaneously with the soil mesh. The motivation for running a 2-D site response analysis rather than a more typical 1-D site response analysis is that the free-field lateral spreading problem involves an inherently two-dimensional response due to the presence of the slope and river channel.

Separate input parameters for the PDMY material were selected for loose and dense clean saturated Nevada sand with relative densities of 35% and 80%. Some of the model inputs were measured (shear wave velocity, permeability), others were estimated from relative density (friction angle), and the remaining parameters were based on the suggestions of the constitutive model developer (Yang et al. 2003) and modified slightly to better match behavior observed in many laboratory tests. Hence, we did not carefully calibrate the constitutive model parameters to minimize the mismatch between experimental measurements and computations, but rather made reasonable estimates of the input parameters from the outset and subsequently observed differences between experiments and computations. The procedure we adopted for estimating the inputs is similar to the procedure one might adopt based on geotechnical data that is often obtained from a site investigation (i.e., penetration resistance, shear wave velocity, visual classification).

The low-strain shear modulus is defined by $G_{\max} = G_r (p'/p_{\text{ref}})^d$, where G_r , p , p_{ref} , and d represent the reference shear modulus, effective confining pressure, reference mean effective confining pressure, and pressure dependent coefficient. The value of p_{ref} was set to 100 kPa and d was set to 0.5. Note that $G_{\max} < G_r$ for the loose sand since $p < p_{\text{ref}}$ and $G_{\max} > G_r$ for the dense sand since $p > p_{\text{ref}}$. The value of G_r was chosen so that the G_{\max} value matched the value computed using $G_{\max} = \rho * v_s^2$ with the shear wave velocities measured in the centrifuge tests (~ 180 m/s for loose sand and ~320 m/s for dense sand). The model is configured so that the number of yield surfaces and plastic modulus associated with each yield surface can be adjusted to match a modulus reduction (i.e., G/G_{\max}) relationship. For this study the EPRI (1993) curve for sands at depths ranging from 6 m to 15 m was input to the model. The high-strain portion of the modulus reduction curve was adjusted to provide the desired effective friction angle. The effective peak friction angle was 38° for the dense sand and 32° for the loose sand. The prototype permeability of the sand was taken as the measured values for Nevada sand, increased by the scaling factor N (centrifugal acceleration) to account for the difference in scaling of diffusion and dynamic processes (Kutter 1995). Lastly, the calibration constants controlling the liquefaction-induced cyclic shear strain, the pore water pressure

buildup (contraction) rate, the dilation tendency, and the phase transformation angle were estimated using the guidelines by Yang et al. (2003), and then further calibrated to approximate the expected cyclic resistances of the Nevada sand under simple shear loading conditions. The calibration constants were adjusted to match liquefaction triggering behavior for the loose sand based on laboratory test data summarized by Kammerer et al. (2000), and cyclic mobility behavior for the dense sand by comparison with laboratory results by Wu (2002). The loose sand model was calibrated so that the soil: 1) reached about 5% single-amplitude shear strain after initiation of liquefaction ($r_u \sim 100\%$) for loose sand; and 2) had a cyclic stress ratio, CSR, against triggering of $r_u \sim 100\%$ in 10 uniform cycles of about 0.12. The dense sand model was calibrated so that it reached 1% shear strain after 10 uniform cycles of CSR=0.24, which is consistent with relations presented by Idriss and Boulanger (2006).

The PIMY material for clay includes 7 major parameters, where the volumetric stress-strain response is linear-elastic and independent of the deviatoric response with a Von Mises type yield surfaces. The low-strain shear modulus was set based on measurements of shear wave velocity in the clay and empirical correlations to undrained shear strength. The undrained shear strength (s_u) was 33 kPa and 22 kPa for DDC01 and DDC02, respectively, and was measured with a small hand vane shear device following spin-down of the centrifuge following testing.

The properties of the soil elements used in the FE model are listed in Tables 3.

Table 3. Input FE analysis baseline case parameters for (a) sand (b) clay.
(a) Properties of sand material

Model Parameters	Loose Nevada Sand	Dense Nevada Sand
------------------	-------------------	-------------------

Mass density (Mg/m ³)	1.9 ⁴	2.0 ⁴
Reference shear modulus G _r (kPa)	6.4e ⁴	7.5e ⁴
Reference soil skeleton bulk modulus B _r (kPa) ^c	2.0e ⁵	2.5e ⁵
Reference confining stress p (kPa)	100	100
Friction angle	32	38
Phase transformation angle	27	15
Contraction constants c	c=0.2	C=0.002
Dilation constants d1, d2	d1=0.4 d2=2	d1=0.002 d2=1
Liquefaction induced strain constants liq	liq1=10 liq2=0.2 liq3=1	liq1=5 liq2=0.0 liq3=0
Number of yield surfaces	11	11
Modulus reduction curve ^a	EPRI (1993) ^a	EPRI (1993) ^a
Permeability (m/s)	0.00007·N ^b	0.00003·N ^b
Combined bulk modulus (kPa) ^c	4700000	4700000

(b) Properties of clay material

Model Parameters	Bay Mud s _u =33kPa(DDC01)	Bay Mud s _u =22kPa(DDC02)
Mass density (Mg/m ³)	1.6	1.6
Reference shear modulus G _r (kPa)	5e4	1.5e4
Reference bulk modulus B _r (kPa)	2.5e5	7.5e4
Undrained Shear Strength (kPa)	33	22
Peak shear strain	0.1	0.1
Reference confining stress p (kPa)	100	100
Friction angle	0	0
Pressure depend coefficient	0	0
Permeability (m/s)	10 ⁻⁸ ·N ^b	10 ⁻⁸ ·N ^b
Solid-fluid mix bulk modulus (kPa)	4.7e6	4.7e6

^a The yield surfaces and hardening parameters were adjusted to match the input modulus reduction curve.

^b N is the centrifuge spinning g-level.

^c Soil skeleton bulk modulus is for the skeleton only, and combined bulk modulus is for the solid/water mixture, and was computed as B_f/n, where B_f is the bulk modulus of water (2.2x10⁶kPa) and n is porosity.

PILE AND SUPERSTRUCTURE PROPERTIES

The piles, pile cap, and superstructure were modeled using elastic beam-column elements having the dimensions and properties listed in Tables 1 and 4. The pile cap was modeled using a box of extremely stiff (essentially rigid) beam column elements masses lumped at the nodes. The pile-to -cap connection was modeled as rigid in rotation, and the displacement degrees of freedom of the node at the top of the pile were constrained to be the same as the matching node on the pile cap. The superstructure was approximated as a concentrated mass of 355 tonne at the center of gravity for the actual mass. The structure columns were modeled as a uniform flexural stiffness (EI) that was chosen to produce fixed-base natural periods that

equaled the measured values. The three-by-two group of piles was represented by three piles, each having twice the axial, bending, and cap connection stiffness of a single pile.

Table 4. Properties of piles and superstructure

Record No.	E (kPa)	I (m ⁴)	A (m ²)	Mass (ton)
Piles	2e8	0.01	0.1	765
Superstructure	2e8	0.01	0.1	355

SOIL SPRINGS ON PILES

The soil springs that connect the structural model to the 2-D soil mesh were modeled using zero-length elements with the nonlinear p-y (lateral resistance), t-z (shaft friction) and q-z (tip resistance) materials described in Boulanger et al. (1999) and Curras et al. (2001). The mean effective stress from the free-field site response analysis is input to the p-y materials, and their capacity is degraded as excess pore pressure develops due to liquefaction according to the equation $p_{ult_liq} = p_{ult} \cdot (1 - r_u) + p_{res} \cdot r_u$. The p_{res} value at $r_u = 1$ is intended to represent the p-y capacity for fully-liquefied sand that is often represented using a p-multiplier that is applied to the drained capacity (e.g., Brandenberg 2005). This formulation captures not only the development of liquefaction, but also the cyclic mobility behavior following liquefaction that has been observed in many laboratory tests. Hence, when the free-field site response simulation induces large shear strains in the sand, the excess pore pressure ratio transiently reduces, and the p-y capacity transiently increases. This is part of the cause of the inverted s-shaped p-y behavior observed in many studies (e.g., Wilson et al. 2001, Tokimatsu et al. 2001). An additional increment of shear strain arises from interaction between the soil and pile, and this feature of behavior is only indirectly captured by setting a non-zero value for the residual capacity of the p-y material. A more recent material model by Varun (2010) also incorporates this near-field effect. The capacities and backbones of the p-y springs on the piles were based on American Petroleum Institute (API 1993) recommendations for sand and Matlock's (1970) recommendations for clay. The soil properties used to compute the capacities (p_{ult}) of the springs were the same as used for the soil models. The stiffness and capacity of the p-y springs depend on the effective stresses in adjoining 2-D soil mesh, thereby approximately accounting for the effect that liquefaction in the free-field soil has on the subgrade reaction. The residual capacity of the p-y springs is 10% of the drained capacity for springs in loose sand, and is 50% of the drained capacity for springs in dense sand. Details on the formulations are given in Boulanger et al. (1999).

The t-z spring capacities (t_{ult}) were computed for clay using the α method (shaft friction, $f = \alpha s_u$) with $\alpha = 1$ and for sand using $f = \sigma_v' K_o \tan \delta$ with $K_o = 0.4$ and $\delta = 24$ degree for loose sand and 30 degree for dense sand. The stiffness and capacity of the t-z materials for sand depend on the effective stresses in adjoining 2-D soil elements, thereby approximately accounting for the effect that liquefaction in the free-field soil has on the shaft friction (details in Boulanger et al. 2003). The backbones of the springs approximated the relation proposed by Reese and O'Neill (1988) for piles in clay, and by Mosher (1984) for piles in sand. The ultimate resistance of t-z material was reached when tip displacement is about 0.5% of pile diameter ($z_{ult} = 0.005 \cdot D_{pile}$).

The drained end-bearing resistance for the sand layer was represented using the bearing capacity factors given by Meyerhof (1976). The ultimate resistance q_{ult} is calculated as $q_{ult} = N_q \cdot \sigma_{v,t}'$, where $\sigma_{v,t}'$ is the effective vertical stress at the pile tip elevation, and the bearing factor, N_q , is often tabulated in a Figure for a range of friction angles, and embedment depths. In the FE model, $N_q^* = 300$ corresponds to an effective friction angle of 38° for the dense sand at the pile tip. The backbone of the q-z relations was modeled after Vijayvergiya's (1977) relation for piles in sand. The stiffness of the q-z materials was set such that the ultimate resistance was reached when tip displacements were about 2.5% of the pile diameter ($z_{ult} = 0.025 \cdot D_{pile}$) based on the stiffer range of Randolph's (1991) recommendations on the initial stiffness of those springs to account for dynamic shaking effects.

The soil springs for lateral loading between the pile cap and the clay crust based on conventional earth pressure theories presented by Brandenberg et al. (2005) and summarized in Table 5. The total crust load consists of passive force on the upslope face, forces on the pile segments between the bottom of the pile cap and the bottom of the crust, and friction along the sides and base of the pile cap. The residual resistance of the lateral soil spring with gapping was set equal to the sum of the side and base friction based on the observation that contact along these surfaces would likely be maintained during upslope movement of the pile cap through an open gap.

Table 5. Estimation of crust load (after Brandenberg et al. 2005)

Test	Passive Force (kN)	Pile Segment Force (kN)	Side Friction (kN)	Base Friction (kN)	Total Crust Load (kN)	Peak Measured Crust Load (kN)
DDC01	2600	2160	650	680	6090	6150

DDC02	2090	1540	480	170	4280	4330
-------	------	------	-----	-----	------	------

Radiation damping for the piles and pile cap were approximated using the dashpot components of the lateral soil springs. When using soil springs as connections to a 2-D soil mesh, there will be some radiation of wave energy from the piles to the soil continuum. The large out-of-plane thickness of the soil continuum for these centrifuge models means that the wave energy transmitted from the piles to the 2-D mesh is smaller than would occur for 3-D conditions, so the dashpots approximate the additional wave energy dissipation. The dashpots are applied to the elastic (i.e., far-field) component of the nonlinear soil springs (Wang et al. 1998), with the dashpot coefficients based on the approximation by Berger et al. (1977) with elastic properties that are consistent with the elastic component of the soil springs. The Berger et al. (1977) frequency-independent approximation is reasonably consistent with the frequency-dependent radiation damping relation suggested by Makris and Gazetas (1993) for the frequency range of interest. The radiation damping relations were formulated for uniform elastic soil profiles, and not for layered profiles with significant nonlinearity like the soil models being analyzed. However, the significant nonlinearity in the hysteretic behavior of the p-y materials introduces additional damping that lessens the relative influence of the radiation damping. Hence, the approximations in assigning radiation damping constants are considered reasonable given the uncertainties involved.

INTERFACE ELEMENTS BETWEEN NONLIQUEFIABLE AND LIQUEFIABLE SOIL

Figure 4(a) shows a displacement discontinuity that formed at the interface between the clay crust and underlying loose sand layer during the centrifuge tests. This displacement discontinuity forms because the shaking-induced excess pore water pressures in the underlying sand causes upward seepage of pore water which is then impeded by the lower permeability clay layer, where it then causes local loosening of the sand beneath the clay and possibly formation of a water film. The physical mechanisms governing the formation of these seepage-induced localizations within slopes were reviewed by Kulasingam et al. (2004), and are currently beyond the capabilities of most FE programs to model accurately (including the PDMY model). To indirectly incorporate the effects of void redistribution on weakening of the interface between the sand and clay, a sequence of zeroLength elements parallel to the direction of the slope was connected between the sand and clay (rigid links were used in the perpendicular direction). The interface elements used herein [Fig 4b] were

essentially rigid-plastic and were coupled (scaled proportionately) to the effective stresses in the underlying sand elements, such that their shear capacities were equal to the drained shear strength of the loose sand before liquefaction ($r_u=0$) and to a fraction of the drained sand strength after liquefaction ($r_u=1$). An interface residual strength of 3 kPa was used for the baseline analyses, and the sensitivity of the analyses to this parameter was evaluated through sensitivity studies. The deformed FE mesh in Figure 2-b illustrates the displacement discontinuity between the clay layer and the underlying loose sand layer that is accommodated by the interface elements.

CONTAINER AND BOUNDARY CONDITIONS

The flexible shear beam model container consists of five essentially rigid rings composed of either stainless steel (bottom two rings) or aluminum (upper three rings) separated by soft rubber material that permits the container to deform as a shear beam. The shear beam container is designed to be very flexible relative to a nonliquefied soil column to minimize the influence of container stiffness (Elgamal et al 2005). However, the mass and stiffness of the container were both deemed important for this study since the liquefied soil profile is anticipated to have very little stiffness. The three-dimensional model container was transformed into two dimensions in the FE model by adjusting the mass density and stiffness of the elements to provide the measured mass and stiffness values for the container. The two-dimensional approximation of the container was specified to match the total mass and lateral stiffness (and hence natural periods) of the actual container. The container was modeled using two-dimensional linear elastic isotropic elastic materials in quad elements, and did not permit drainage from the soil. The properties are listed in Table 5.

Table 5. Properties of the centrifuge container

Aluminum	Young's modulus E (kPa)	Poisson's ratio	Mass density (Mg/m ³)	Height (m)
Ring 1	68900	0.3	2.084	4
Rubber	4654	0.4	4.966	0.4
Ring 2	68900	0.3	2.468	4
Rubber	2605	0.4	2.67	0.4
Ring 3	68900	0.3	2.468	4
Rubber	3192	0.4	3.263	0.4
Ring 4	68900	0.3	4.676	4
Rubber	3192	0.4	3.263	0.4
Ring 5	68900	0.3	5.87	4
Rubber	1771	0.4	3.602	0.4

The surface of the clay and the sand within the channel were free to drain, while all other soil boundaries were impervious. Pore water pressures for the nodes along the free drainage surfaces were set to the hydrostatic values from the water in the channel. The pressures from the water were also modeled as distributed (hydrostatic) pressures along the channel, with hydrodynamic effects reasonably assumed to be negligible for the slope involved.

ANALYSIS SEQUENCE

The sequences of the FE analysis include the following steps: 1) The soil and container meshes were built, and soil permeability was set to a constant value for all layers for fast consolidation under gravity loads, the materials were assigned elastic properties, and then static gravity of the model self weight and hydrostatic pore water pressure from the open water channel were applied to provided the initial soil stress-states for the subsequent analysis; 2) the initial soil deformations from gravity stage were reset to zero, and pile, superstructure and soil spring elements were implemented into the FE model, also structural and pile cap weight were applied as nodal vertical loads, and the material response was set to plastic mode (iteration was required to reach equilibrium upon switching from elastic to plastic mode as the internal material constants updated); 3) soil permeability was set back to the appropriate values (Table 3), soil and springs materials were updated to plastic stage, and dynamic excitations were applied. A sequence of four motions was applied to each model, and enough time was permitted between shakes to allow excess pore pressures to dissipate. The recorded base motions from the centrifuge tests were applied to the fixed nodes at the base of the soil and container meshes using the UniformExcitation command in OpenSees.

The Newmark method was used to integrate the dynamic response with $\gamma=0.6$ and $\beta=0.3025$ for convergence. The penalty method was used for imposing equal-degree-of-freedom constraints between nodes. Rayleigh damping was included, with the mass proportional damping (a_m) and stiffness proportional damping (a_k) set as $a_m=0.00$ and $a_k=0.006$ according to the estimated first mode frequency and assuming 3% damping for the soil-pile-structure system. The actual damping levels were dominated by hysteretic damping in the nonlinear materials for these analyses, while the above numerical damping sources helped to minimize convergence problems at lower levels of shaking.

COMPARISONS OF RECORDED AND COMPUTED SYSTEM RESPONSES

A total of eight cases (two models, four earthquakes) were analyzed using the single baseline set of parameters in Table 2. Computed responses are in reasonably good agreement with their recorded counterparts for all eight cases. Detailed time series of recorded response for centrifuge model DDC01 ($T_{\text{fixed-base}} = 0.8$ s) are presented for a large Kobe motion ($a_{\text{max,base}} = 0.67$ g) as an example of the agreement between recorded and predicted responses.

The recorded and computed soil and structural responses were compared in Figures 5, 7 and 8. The comparisons included time series of soil, pile and superstructure accelerations, excess pore water pressure in the sand, clay crust and pile cap displacements, lateral loads on pile cap, pile head bending moments, and bending moment distribution along the piles.

SOIL, PILE AND STRUCTURE RESPONSES

Figure 5-a compared computed and recorded acceleration time series, which from bottom up showed accelerations of the dense sand, loose sand, clay crust, pile cap and superstructure mass. The FE computed accelerations captured the progressive amplification of the low frequency contents and de-amplification of the high frequency contents of the input motions through the soil profile, but missed some of the acceleration spikes caused by fluctuations in the excess pore water pressure. The measured fluctuations are pronounced, with r_u becoming negative during some loading cycles for the loose sand, and the excess pore pressure ratio computed by the constitutive model exhibited a weaker cyclic mobility response. The measured behavior is consistent with observations of loose Nevada sand from other centrifuge model studies (e.g., Brandenberg et al. 2005), and is supported by cyclic mobility behavior measured in many laboratory studies (e.g., Boulanger and Truman 1996).

Figure 5-b displayed the computed and recorded time series of excess pore water pressure ratios r_u in the dense and loose sand, and lateral displacements of the pile cap and clay crust. The dynamic FE computed results reproduced the pore water pressure build-up reasonably well, with a slight overall tendency to overestimate r_u in the dense sand in the early stage of shaking and to underestimate soil dilatancy (i.e., transient drops in r_u). The less dilative behavior of the loose sand in the FE model also contributed to the weaker dynamic oscillations of the computed crust displacements during shaking. The computed dynamic pile cap displacements and crust displacements both underestimated their recorded counterparts by 12% and 20%, respectively. The recorded permanent crust displacement kept increasing

significantly after shaking, and the post-shaking crust movement is attributed to the upwardly seeping pore water accumulating at the interface between crust and loose sand. The computed crust displacement stayed stable after shaking since the residual strength of the interface element and loose sand elements in the FE model were set larger than the static shear stress caused by the slope, so it held the crust in equilibrium after the dynamic excitation stopped. These observations indicate that the actual shear strength at the interface in the centrifuge model was lower than the static driving shear stress, at least for some time following shaking while pore pressures dissipated at the interface. This feature of behavior is difficult to capture numerically using the interface elements adopted in this study because of numerical instabilities that can arise when static driving stresses exceed strengths.

LATERAL LOADS ON PILES

There are two major lateral loads acting on the pile cap in a laterally spreading ground during earthquake shaking, namely, inertial loads due to the accelerations of the pile cap and superstructure masses, and the lateral spreading soil load (crust load) due to the large lateral displacement of the nonliquefiable crust. Figure 6 shows the free body diagram of the pile cap during lateral spreading and earthquakes, where the total lateral load on the pile cap (the total shear at the pile head) is equal to the sum of inertial and the crust loads.

$$V = P + I_{ss} + I_{cap}, \quad (1)$$

FE computed and centrifuge recorded time series of bending moment and total shear at the pile head, crust load on the pile cap, total inertial load (cap inertia plus superstructure inertia), together with the ground surface displacement and r_u in the middle of loose sand are compared in Figure 7 for DDC01 in the large Kobe motion. The FE computations agree well with the centrifuge recordings in terms of the predominant periods and magnitudes of the lateral loads, as well as the phasing of inertial and crust loads. The peak values in the response parameters tend to be in phase and reasonably consistent. The ultimate values (peak denotes a local maximum, while ultimate denotes the largest value during the shaking sequence) predicted by the FE computations sometimes occur during different cycles than the measured quantities, but the computations predict the timing of the peaks quite well. The FE model agreed with the recordings in showing that peak pile head bending moments occurred at the timings of peak crust loads. The cycles that produced peak crust loads were associated with the strain-hardening responses and transient drops in r_u in the underlying loose sand layer, when the loose sand was temporarily stiff and strong and held the pile group in place as

the crust slipped past the pile group down slope. A local peak in the inertia load occurred simultaneously with this dilatancy-induced response.

Comparison of recorded and computed bending moment distribution with depth along the piles at the critical loading cycle (timing of maximum total lateral load) was plotted in Figure 8. The FE computation is most accurate at the pile cap connection, and deviates a bit from the measured bending moments deeper in the profile, though the prediction is reasonably consistent with the measurements.

Detailed results were presented for the large Kobe motion for DDC01, but generally good agreement between computed and recorded time series of lateral loads on the pile cap and pile head bending moments were obtained for all eight cases (four events, two structures). For example, recorded and computed time series of total shear on the pile head for DDC01 in all four motions were plotted and compared in Figure 9, which showed that for all four motions, the FE model reproduced the recorded loads quite well.

The maximum structural responses were also compared between the recorded and calculated values for the eight earthquake events. The maximum FE computed system responses were plotted against the recorded peak values for all four motions in Figure 10. The system responses include pile and structure accelerations, and total shear and bending moment at the pile head. The solid dots are for DDC01 and hollow dots are for DDC02; the triangles are the three Santa Cruz motions and the round dots are the large Kobe motion. Overall, computed maximum responses were in reasonably good agreement with their recorded counterparts with errors less than 30%. It also showed that structural responses increased about linearly with a_{\max} for the three scaled Santa Cruz motions (the first three data points), and jumped to a much higher value from the large Santa Cruz motion (the third data point) to the large Kobe motion (the fourth data point) even at similar a_{\max} , which reflected the influence of the frequency content of input base motion.

SENSITIVITY STUDY OF THE FINITE ELEMENT MODEL

The purpose of this sensitivity study is to understand the influence of input variables on some key output variables such as total shear forces on the pile cap, pile head bending moment, and clay crust displacement, etc. This is important for understanding which input parameters most influence system responses, and therefore must be carefully characterized, and which have little effect on the analysis results.

The following input variables were each assigned a range of values for sensitivity study:

- The strength (p_u) of the interface elements.
- The parameters of the p-y springs on the pile cap.
- The out-of-plane thickness of soil.

SENSITIVITY TO STRENGTH OF THE SOIL LAYER INTERFACE ELEMENTS

Sensitivity of the computed maximum lateral loads on the pile cap to the strength of the interface elements between the top clay crust and the underlying liquefiable sand layer for DDC01 during the large Kobe earthquake is presented in Figure 11, where the interface element strength (p_u) is expressed as a fraction of the loose sand layer's drained shear strength (s_d). The drained shear strength (s_d) of the loose sand was calculated as 30kPa based on the initial vertical effective stress at the interface and friction angle of the loose sand. The ratio of $p_u/s_d = 0.2$ is for the baseline case, where the strength the interface elements was equal to 6kPa, with the other p_u/s_d ratios varying from 0.1 to 1.0.

The maximum crust load decreased nearly linearly with increasing p_u of the interface elements. As p_u increased, the computed maximum crust load decreased because stiffer interface elements led to smaller crust displacements and thus smaller crust load on the pile cap. For the case of $p_u / s_d < 0.5$, the ultimate crust load P_{ult} was mobilized since the interface sliding caused the relative lateral displacement between the pile cap and the crust to be larger than y_{ult} of the p-y springs; for the case of $p_u / s_d > 0.5$, P_{ult} was not mobilized due to the small interface sliding (less than 1% of the crust thickness, thus smaller than y_{ult}), but a significant fraction of crust load was still mobilized due to the ground lurch.

The maximum inertial load did not change much with interface element strength p_u , but the maximum total shear decreased considerably with increasing p_u . Inertial and crust loads were more in phase when large displacement discontinuities occurred at the interface, but more out of phase when no slip was permitted. The change of loading mechanism caused by interface sliding was discussed in greater details in Chang (2007) using equivalent-static pushover analyses.

Results of additional sensitivity studies are presented in Chang (2007), including the effects of permeability, input motions, and mesh refinements.

SENSITIVITY TO THE OUT-OF-PLANE THICKNESS OF SOIL MESH

The effect of the out-of-plane thickness of soil mesh was studied by repeating analyses with the soil thickness equal to 1000 m (large massive soil) and 50 m (the real thickness of centrifuge model container for DDC01 in the large Kobe motion). It showed that with the same interface element properties, the difference in key output variable caused by the out-of-plane soil thickness are all within 3%. Therefore, as long as the out-of-plane thickness of soil mesh makes the soil massive enough compared to the piles and structures to generate a free-field site response, changes in the out-of-plane soil thickness do not significantly affect the system responses.

LIMITATIONS OF THE FINITE ELEMENT MODEL

Differences between the computed and recorded data could be caused by the uncertainty in the analytical model parameters (e.g., soil constitutive model parameters, strength of the interface elements; load transfer between the piles and the clay crust due to the gap formation/closure around the piles; etc.), differences between the three-dimensional physical models and the two-dimensional representation (e.g., omission of soil densification due to previous shaking events; omission of the clay cracking during ground oscillation; 3-D soil-container and soil-pile interactions; etc.), or limitations of the numerical modeling approach in general. However, agreement between the FE computations and the recorded data are reasonable considering that a single set of input parameters was used to define the models for a wide range of input ground motions.

SUMMARY

A 2-D FE dynamic model of soil-pile-structure system was developed calibrated and evaluated against a set of centrifuge model tests involving pile-supported-structure in a soil profile (gently sloping 5-m thick clay overlying saturated loose sand overlying saturated dense sand) that produced liquefaction and lateral spreading ground during earthquakes. Four different earthquake events (scaled Kobe and Santa Cruz earthquakes with $a_{\max} = 0.13 - 0.7 \text{ g}$) were performed on two FE models (superstructure $T_{\text{fixed-base}} = 0.3 \text{ s}$ and 0.8 s). One baseline set of parameters was selected and calibrated against the centrifuge data and used in the dynamic analysis for all eight cases. Computed and recorded responses of the soil-pile-superstructure system were compared for all eight shaking events. Influence of the FE model input variables on computed results was studied to qualify their different significance.

The 2-D FE model developed on OpenSees platform included liquefiable soil elements, elastic beam column elements, nonlinear soil springs, and interface elements. The displacement discontinuity at the clay-loose sand interface was modeled using a set of zero-length interface sliding elements in the FE model. The p-y springs on pile cap were constructed based on the much softer load transfer behavior that accounts for the influence of underlying liquefiable sand on the load transfer in the crust.

The FE model was developed for two purposes: (1) reproduce the experimental results and assist in illustrating the physics and mechanisms of the soil-pile-structural system during complex dynamic loading conditions, and (2) evaluate how sensitive the computed responses are to some input variables, and build the basis for further parametric studies to understand how the observed loading mechanism might be extended to a broader range of conditions.

Good agreement was achieved between the dynamic FE analysis and the centrifuge data for the overall soil and structural responses over the conditions covered in the centrifuge tests. With the same baseline set of parameters, the FE analysis could reproduce the maximum total lateral loads on the pile cap with error less than 10% and the pile head bending moments with error less than 15% on average. The best agreement between computed and recorded results were achieved for the large Kobe motion because the baseline values for two of the more uncertain parameters (residual strength at clay-sand interface, and the soil spring properties on the pile cap) were calibrated against the centrifuge data from the large Kobe motion

Sensitivity studies of the FE model showed that the interface sliding between the crust and underlying loose sand layer had significant effects on the lateral spreading soil load exerted on the pile cap, which contributed significantly to the total lateral load on the pile cap and pile head bending moment during earthquakes.

Considering the complications involved, the FE model was able to capture the important mechanisms of load transfer and to be used as a rational basis for estimating behavior for different conditions. Centrifuge model testing data provided a valuable database for calibrating analytical method for numerical simulations. The comparison of eight cases (two models, four motions) showed the values of evaluating the numerical tool against a wide range of conditions instead of a single set of data.

The centrifuge test data consistently show (and the FE simulations consistently predict) that kinematic loads imposed by lateral spreading and inertia demands caused by ground shaking can act simultaneously. Many design procedures specify that these demands should not be combined in analysis based on the assumption that the peak inertia demands occur near the beginning of shaking before the onset of liquefaction, while lateral spreading occurs later in shaking or after shaking due to liquefaction. However, the test data and dynamic FE analyses consistently show that large inertia demands can occur even after the onset of liquefaction. The dilatancy behavior of the liquefied sand (manifested as sudden drops in pore water pressure in undrained loading) is largely responsible for the large inertia demands after liquefaction during some large cycles.

REFERENCES

- American Petroleum Institute (API)., 1993. *Recommended Practice for Planning, Design, and Constructing Fixed Offshore Platforms*, API RP 2A-WSD, 20th ed., American Petroleum Institute.
- Abdoun, T. and Dobry, R., 2002. Evaluation of pile foundation response to lateral spreading, *Soil Dynamics and Earthquake Engineering*, No 22, 1051-1058.
- Boulanger, R. W., Curras C. J., Kutter, B. L., and Wilson, D. W., 1999. Seismic soil-pile-structure interaction experiments and analyses, *J. Geotech. Geoenviron. Eng.*, Sept. 1999, 750-759.
- Boulanger, R. W., Kutter, B. L., Brandenburg, S. J., Singh, P., and Chang, D., 2003. Pile foundations in liquefied and laterally spreading ground during earthquakes: Centrifuge experiments and analyses, *Report UCD/CGM-03/01*, Center for Geotechnical Modeling, Univ. of California, Davis, CA. <http://nees.ucdavis.edu>.
- Boulanger, R. W., and Tokimatsu K. (Editors) (2005). Seismic Performance and Simulation of Pile Foundations in Liquefied and Laterally Spreading Ground, *Proc., a Workshop*, March 16–18, 2005, Davis, California, USA.
- Boulanger, R. W., Wilson D. W., Kutter, B. L., 1997. Soil-pile-superstructure interaction in liquefiable sand, *Transportation Research Record 1569*, TRB, National Research Council, National Academy Press, Washington D.C., pp. 55-64.
- Brandenburg, S. J., 2005. Behavior of pile foundations in laterally spreading ground, *Ph.D. dissertation*, University of California, Davis.
- Brandenburg, S. J., Boulanger, R. W., Kutter, B. L., and Chang, D., 2005. Behavior of pile foundations in laterally spreading ground during centrifuge tests, *J. Geotech. Geoenviron. Eng.*, 131(11), 1378-1391.

- Brandenberg, S.J., Boulanger, R.W., Kutter, B.L., and Chang, D., 2006. Observations and analysis of pile groups in liquefied and laterally spreading ground in centrifuge tests, *Simulation and Performance of Pile Foundations in Liquefied and Laterally Spreading Ground, GSP 145*, ASCE.
- Brandenberg, S. J., Boulanger, R. W., Kutter, B. L., and Chang, D., 2007. Liquefaction-induced softening of load transfer between pile groups and laterally spreading crusts, *J. Geotech. Geoenviron. Eng.*, ASCE, 133(1), 91-103.
- Brandenberg, S. J., Boulanger, R. W., Kutter, B. L., Wilson, D. W., and Chang, D., 2004. Load transfer between pile groups and laterally spreading ground during earthquakes, in *Proceedings, 13th World Conf. on Earthquake Engineering*, paper 1516, Vancouver, Canada.
- Chang, D., 2007. Inertial and Lateral Spreading Demands on Soil-Pile-Structure Systems in Liquefied and Laterally Spreading Ground during Earthquakes. *Ph.D Dissertation*, Department of Civil Engineering, University of California, Davis.
- Chang, D., Boulanger, R. W., Kutter, B. L., and Brandenberg, S. J., 2005. Experimental observations of inertial and lateral spreading loads on pile groups during earthquakes, *Earthquake Engineering and Soil Dynamics, GSP 133*, ASCE.
- Chang, D., Boulanger, R. W., Kutter, B. L., and Brandenberg, S. J., 2006. Dynamic analyses of soil-pile-structure interaction in laterally spreading ground during earthquake shaking, *Seismic Performance and Simulation of Pile Foundations in Liquefied and Laterally Spreading Ground, GSP 145*, ASCE, pp. 218-229.
- Chang, D., Brandenberg, S. J., Boulanger, R. W., and Kutter, B. L., 2004 (a). Behavior of piles in laterally spreading ground during earthquakes – centrifuge data report for DDC01, *Report No. UCD/CGMDR-04/01*, Center for Geotechnical Modeling, Department of Civil Engineering, University of California, Davis.
- Chang, D., Brandenberg, S. J., Boulanger, R. W., and Kutter, B. L., 2004 (b). Behavior of piles in laterally spreading ground during earthquakes – centrifuge data report for DDC02, *Report No. UCD/CGMDR-04/02*, Center for Geotechnical Modeling, Department of Civil Engineering, University of California, Davis.
- Chang, D., Thaleia Travararou, and Jacob Chacko, 2008. Numerical Evaluation of Liquefaction-induced Uplift for an Immersed Tunnel, *Proceedings of 14th world conference on earthquake engineering*, Beijing, China.
- Curras C. J., Boulanger, R. W., Kutter, B. L., and Wilson, D. W., 2001. Dynamic experiments and analyses of a pile-group-supported structure, *J. Geotech. Geoenviron. Eng.*, July 2001, 585-596.
- Dobry, R., Abdoun, T., O'Rourke, T. D., and Goh, S. H., 2003. Single Piles in Lateral Spreads: Field Bending Moment Evaluation, *J. Geotech. Geoenviron. Eng.*, ASCE, Vol. 129(10), 879-889.

- Elgamal, A., Yang, Z., and Parra. E., 2002. Computational modeling of cyclic mobility and post-liquefaction site response, *Soil Dynamics and Earthquake Engineering*, 22 (2002), 259-271.
- Elgamal, A., Yang, Z., Parra. E., and Ragheb A., 2003. Modeling of cyclic mobility in saturated cohesionless soils, *International J. of Plasticity*, 19(2003), 883-905.
- Elgamal, A., Yang, Z., Lai T., Kutter, B. L., and Wilson D. W., 2005. Dynamic response of a saturated dense sand in Laminated centrifuge container, *J. Geotech. Geoenviron. Eng.*, May 2005, 598-609.
- Gazetas, G., and Dobry, R., 1984. Simple radiation damping model for piles and footings, *J. Eng. Mechanics*, 110(6), 937-956.
- Kammerer, A., Wu, J., Pestana, J., Riemer, M., and Seed, R. 2000. Cyclic simple shear testing of Nevada sand for PEER Center project 2051999. Geotechnical Engineering Research Report UCB/GT/00-01, University of California, Berkeley, California.
- Kulasingam, R., Malvick, E. J., Boulanger, R. W., and Kutter, B. L., 2004. Strength Loss and Localization at Silt Interlayers in Slopes of Liquefied Sand, *J. Geotech. Geoenviron. Eng.*, ASCE, Vol. 130(11), 1192-1202.
- Kutter, B.L., 1991. Dynamic centrifuge modeling of Geotechnical structures, *Transportation Research Record 1336, TRB, National Research Council*, Washington D.C., 24-30.
- Kutter, B.L., 1995. Recent advances in centrifuge modeling of seismic shaking, State-of-the-Art paper, *Proc. 3rd International Conference on Recent Advances in Geotechnical Earthquake Engineering and Soil Dynamics*, St. Louis, MO, April, 1995, Volume II, 927-942.
- Ilnkatharan, M., and Kutter, B.L., 2008. Numerical Simulation of a Soil Model-Model Container-Centrifuge Shaking Table System, *Seismic Performance and Simulation of Pile Foundations in Liquefied and Laterally Spreading Ground, GSP 181*, ASCE..
- Lai, T., Elgamal, A., Wilson, D.W., and Kutter, B.L., 2001. Numerical modeling for site seismic response in laminated centrifuge container, *Proc. 1st Albert CAQUOT Int. Conf.*, Paris.
- Matlock, H., 1970. Correlations of design of laterally loaded piles in soft clay, *Proc. Offshore Technology Conference*, Houston, TX, Vol 1, No.1204, 577-594.
- Matlock, H., Foo, S. H. C. and Bryant, L. M., 1978. Simulation of laterl pile behavior under earthquake motion, *Earthquake Engineering and Soil Dynamics*, Pasadena, California, 600-619.
- Tokimatsu, K., Suzuki, H., and Suzuki, Y., 2001. Back-calculated p-y relation of liquefied soils from large shaking Table tests, *Fourth International Conference on Recent Advances in Geotechnical Engineering and Soil Dynamics*, S. Prakash (ed.), University of Missouri – Rolla, Paper 6.24.

- Wilson, D. W., Boulanger, R. W., and Kutter, B. L., 1999. Lateral resistance of piles in liquefying sand, *OTRC, 99 Conference on Analysis, Design, Construction and Testing of Deep Foundations*, Roesset J. M. Ed., Geotechnical Special Publication No. 88, ASCE, 165-179
- Wilson, D. W., Boulanger, R. W., and Kutter, B. L., 2000. Observed seismic lateral resistance of liquefying sand, *J. Geotech. Geoenviron. Eng.*, ASCE, Vol. 126(10), 898-906.
- Wilson, D. W., Boulanger, R. W., and Kutter, B. L., and Abghari, A. (1995). Dynamic centrifuge tests of pile supported structures in liquefiable sand, *Proc. of the National Seismic Conference on Bridges and Highways—Progress in Research and Practice*, FHWA and Caltrans, San Diego, CA
- Yang, Z., 2000. Numerical modeling of earthquake site response including dilation and liquefaction., *Ph.D. Dissertation*, Department of Civil Engineering and Engineering Mechanics, Columbia University, New York, N.Y.
- Yang, Z., and Elgamal, A., 2002. Influence of permeability on liquefaction-induced shear deformation, *J. Geotech. Geoenviron. Eng.*, July 2002, 720-729.
- Yang, Z., and Elgamal, A., 2005. OpenSees manual for PDMY and PIMY materials, <http://cyclic.ucsd.edu>.
- Yang, Z., Elgamal, A., and Parra, E., 2003. A computational model for liquefaction and associated shear deformation, *J Geotech Geoenviron Eng*, ASCE, 129(12), 1119-1127.

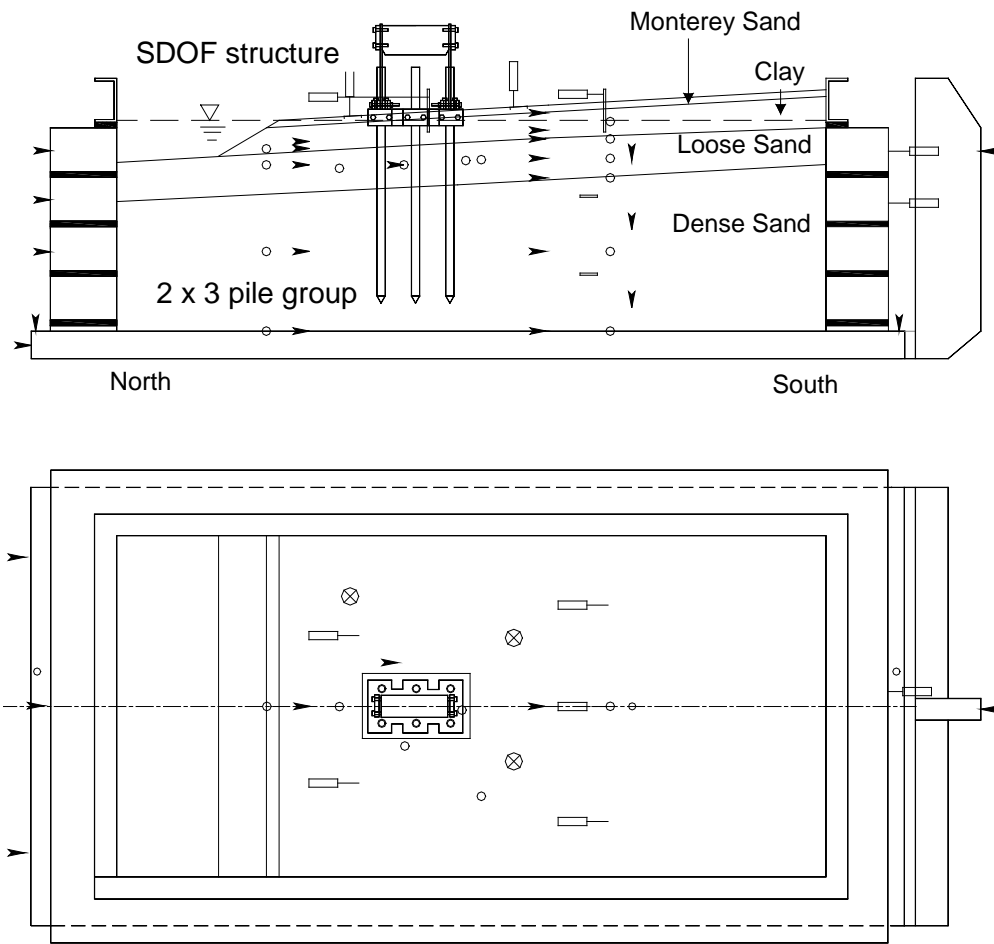


Figure 1. Centrifuge model layouts with approximately 100 transducers per model. (Some sensors omitted from sketch for clarity)

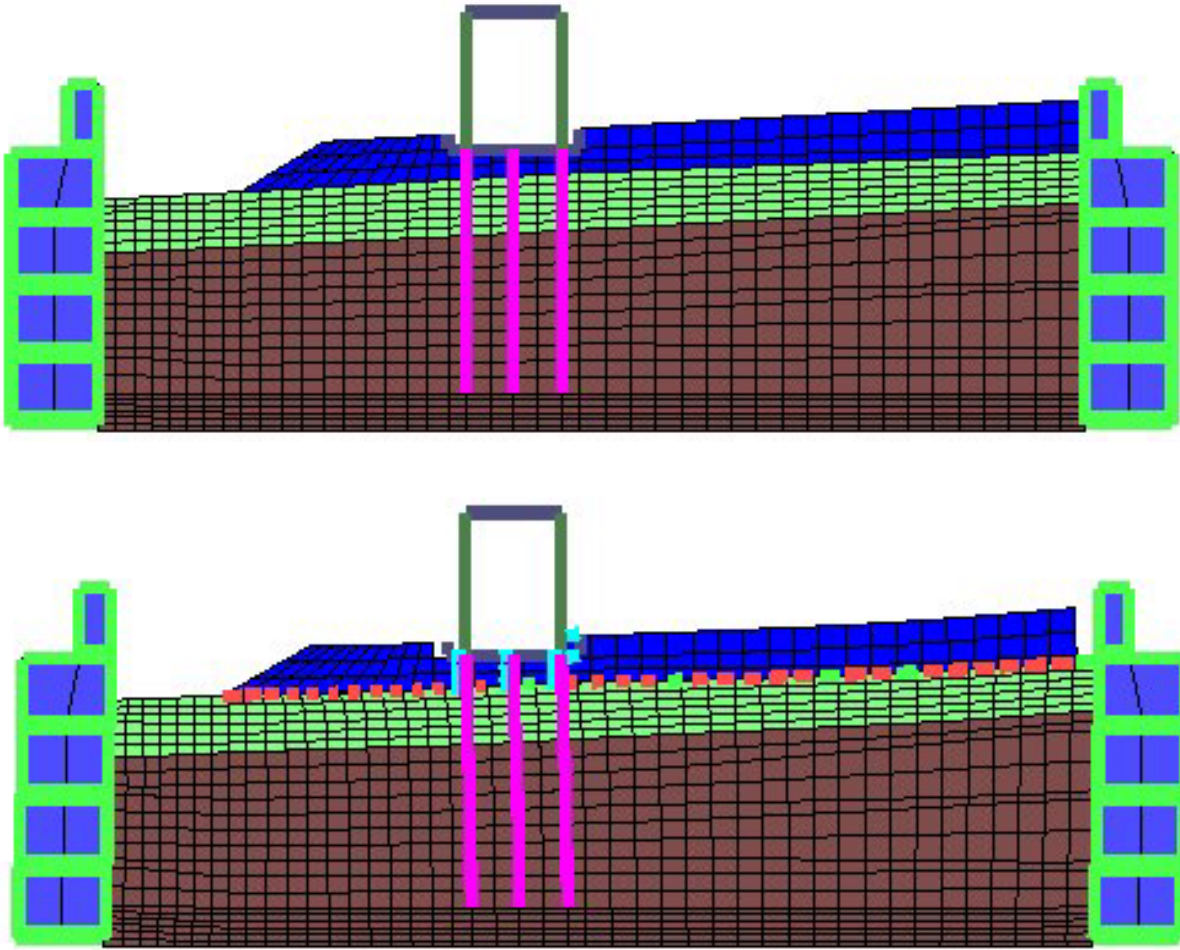


Figure 2. 2D FE mesh (a) undeformed 2D FE mesh, (b) deformed mesh after earthquake shaking.

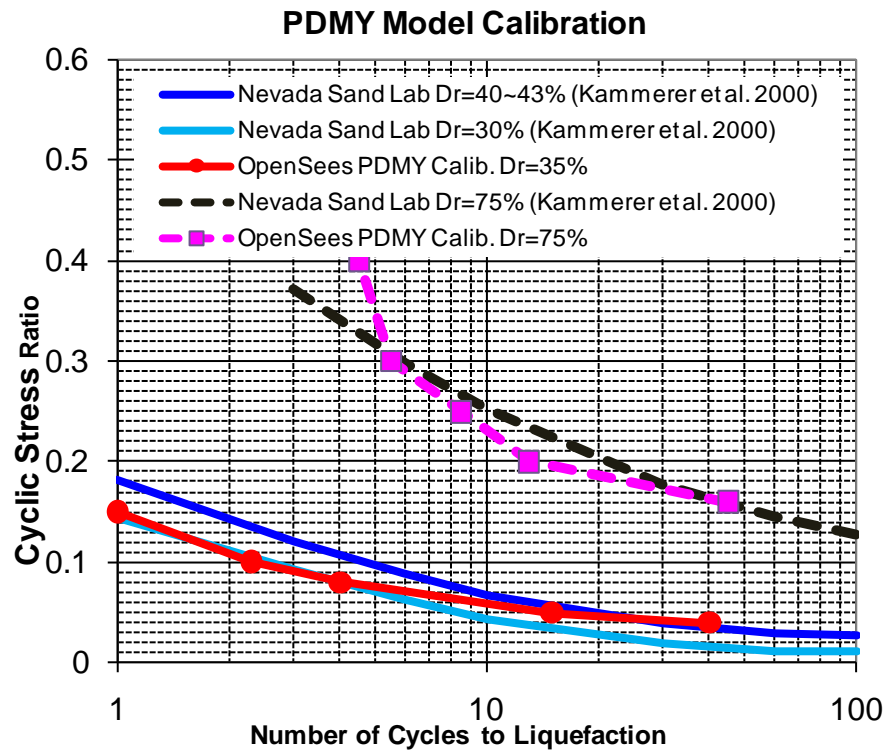
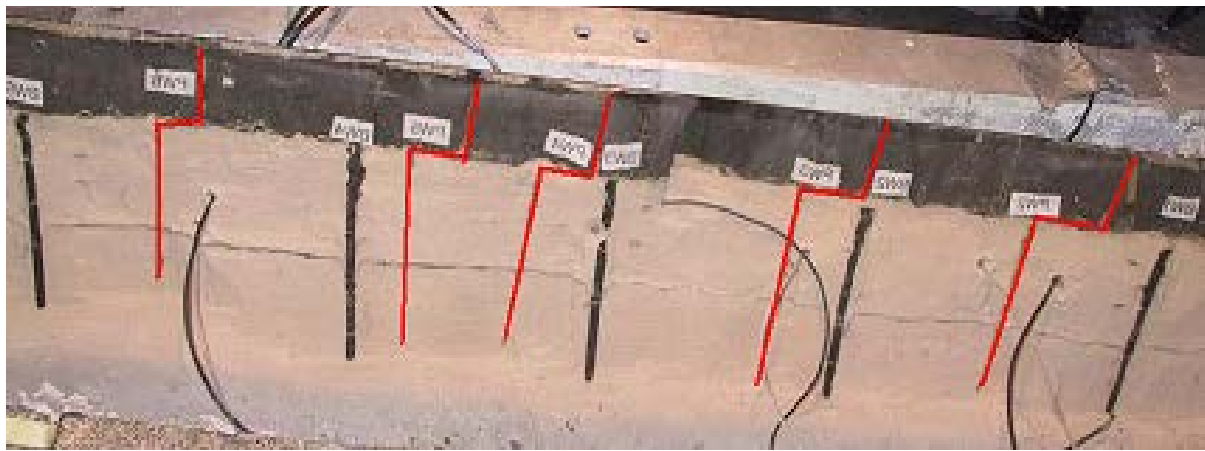


Figure 3. Liquefaction resistance calibration of PDMY material in OpenSees. (compare with data from cyclic simple shear tests by Kammerer et al. 2000)



Before liquefaction

After liquefaction

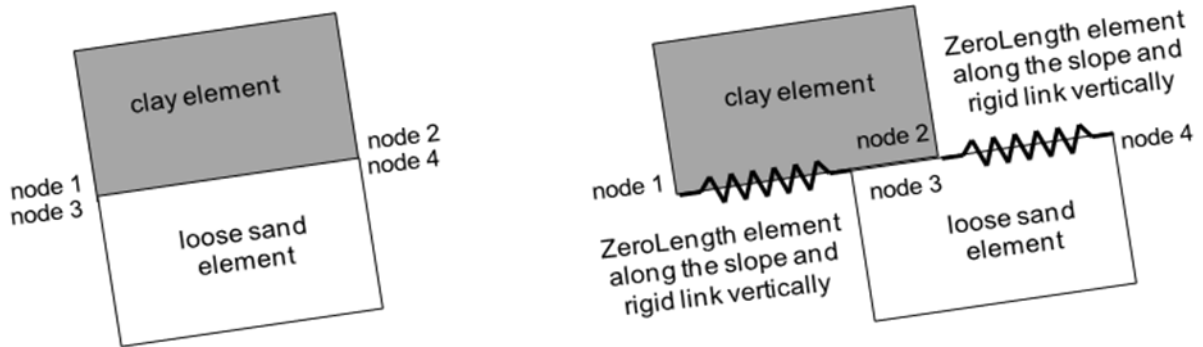
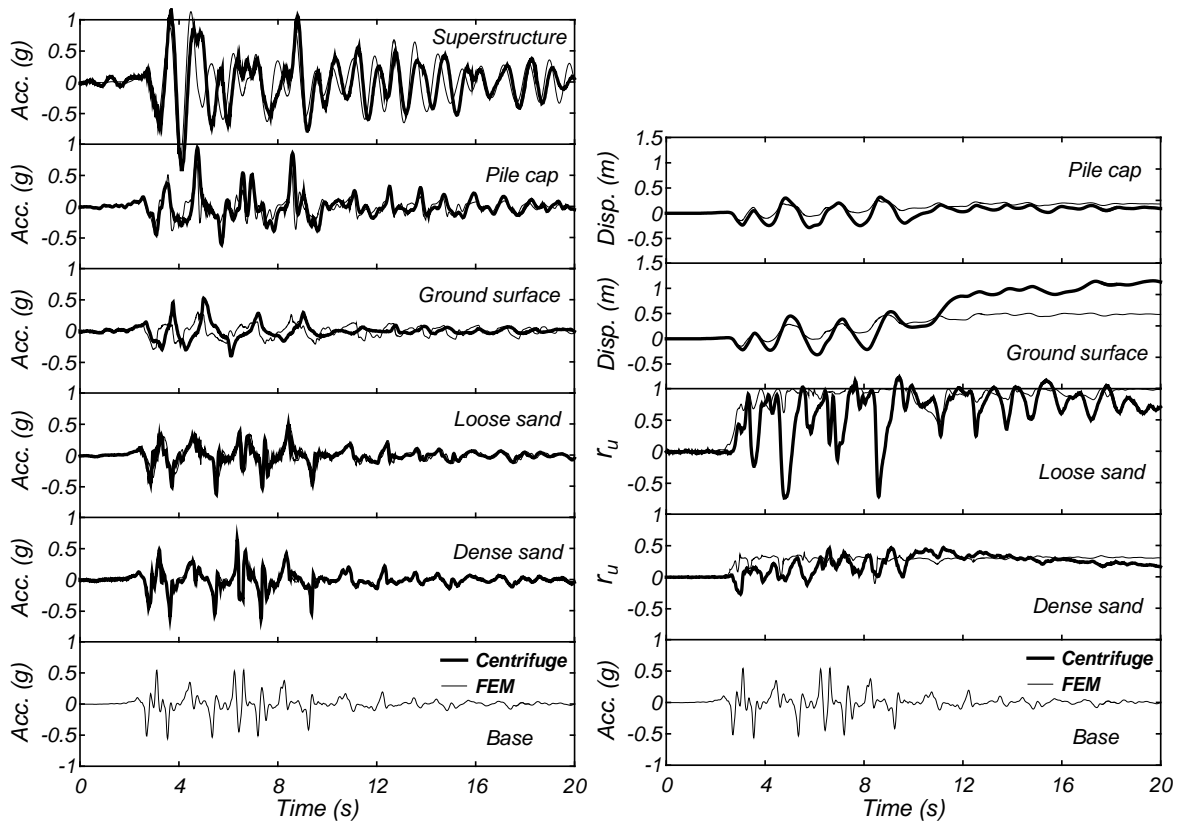


Figure 4. (a) Excavation after shakes showing the displacement discontinuity at the interface between the top clay crust and the underneath liquefied sand layer (paper markers were highlighted in red for clarity, DDC02 model), and (b) interface springs in the FE model.



DDC01 in Large Kobe Motion

DDC01 in Large Kobe Motion

Figure 5. Comparison of recorded and computed (a) soil, pile cap and superstructure accelerations, and (b) pore water pressure in loose and dense sand, crust and pile cap displacements for the $T_{\text{fix_base}}=0.8\text{s}$ structure during the large Kobe motion.

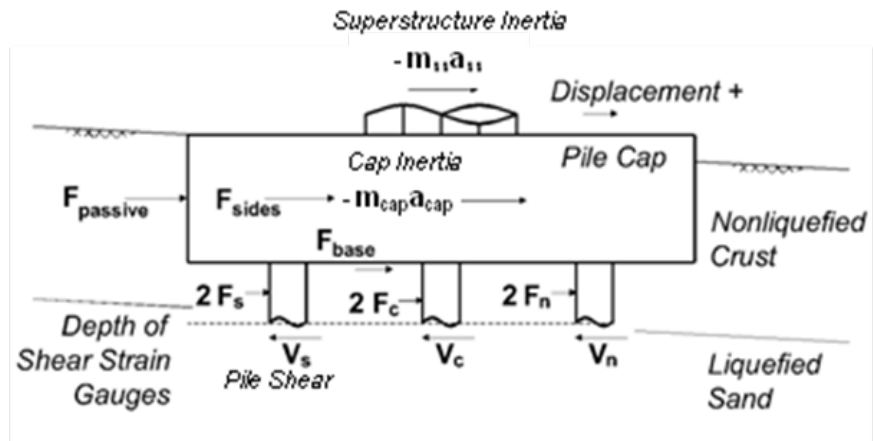
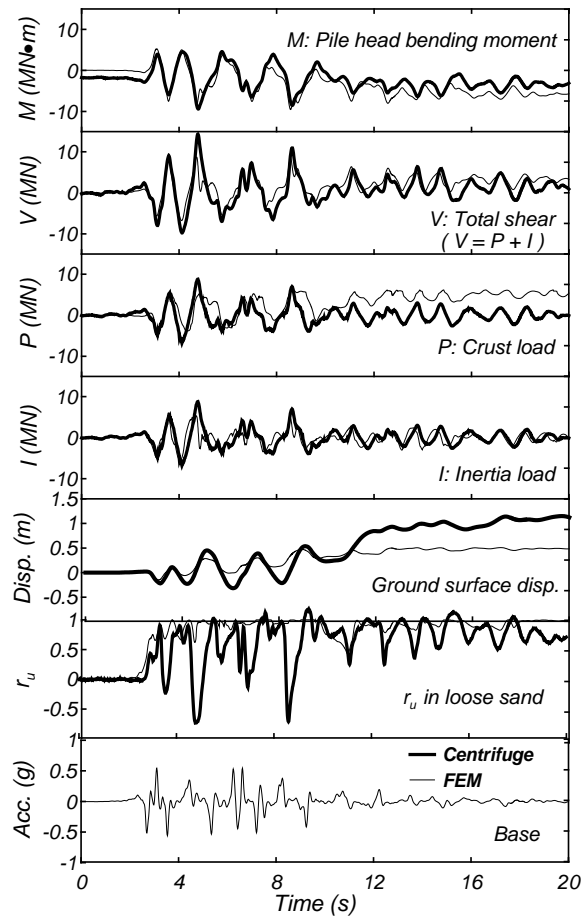
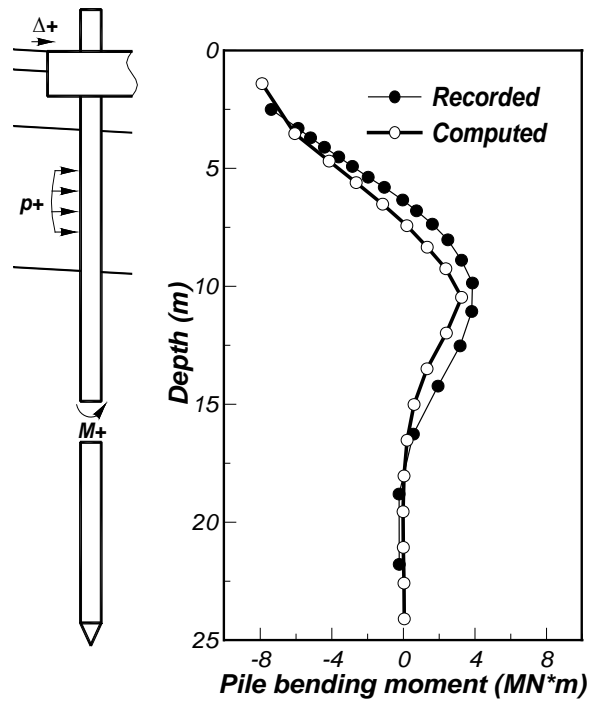


Figure 6. Free body diagram of pile cap during lateral spreading and earthquake.



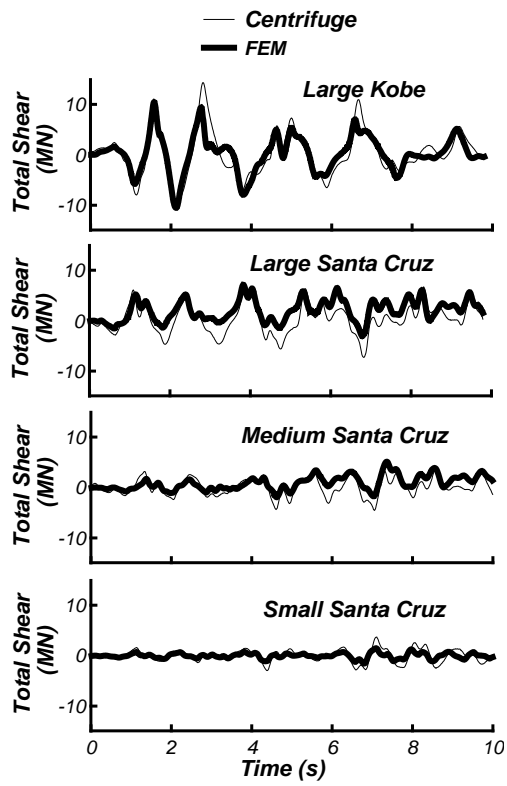
DDC01 in Large Kobe Motion

Figure 7. Comparison of recorded and computed pile head bending moment, lateral loads on the pile cap, ground surface displacement, pore pressure ratio in the middle of loose sand for the $T_{\text{fix_base}}=0.8$ s structure during the large Kobe motion.



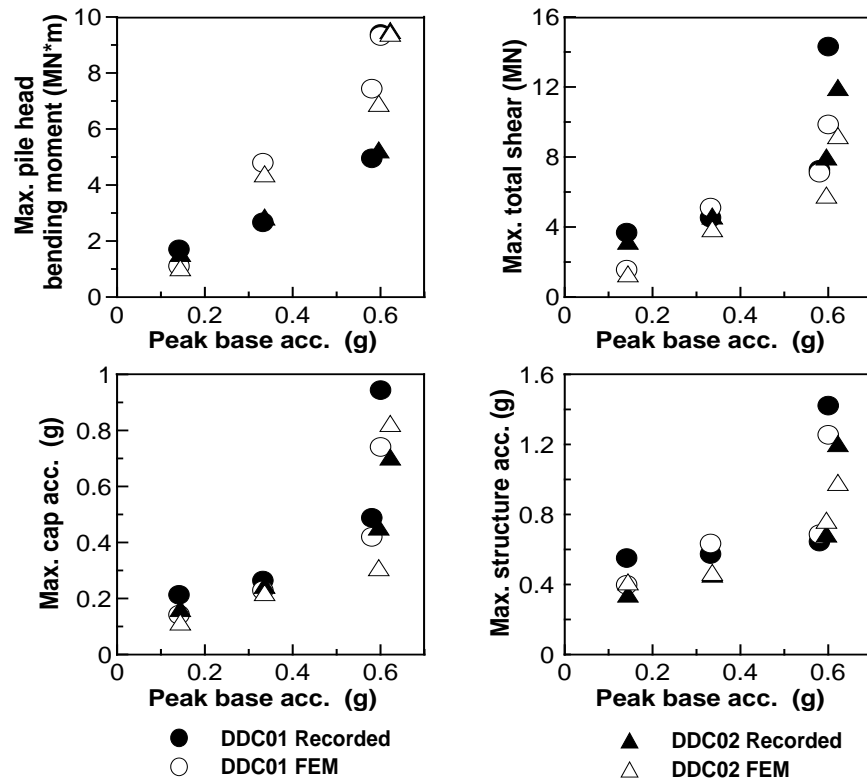
DDC01 in large Kobe motion

Figure 8 Snapshot of recorded and computed bending moment distributions along piles at the critical loading cycles for the $T_{\text{fix_base}}=0.8$ s structure during the large Kobe motion.

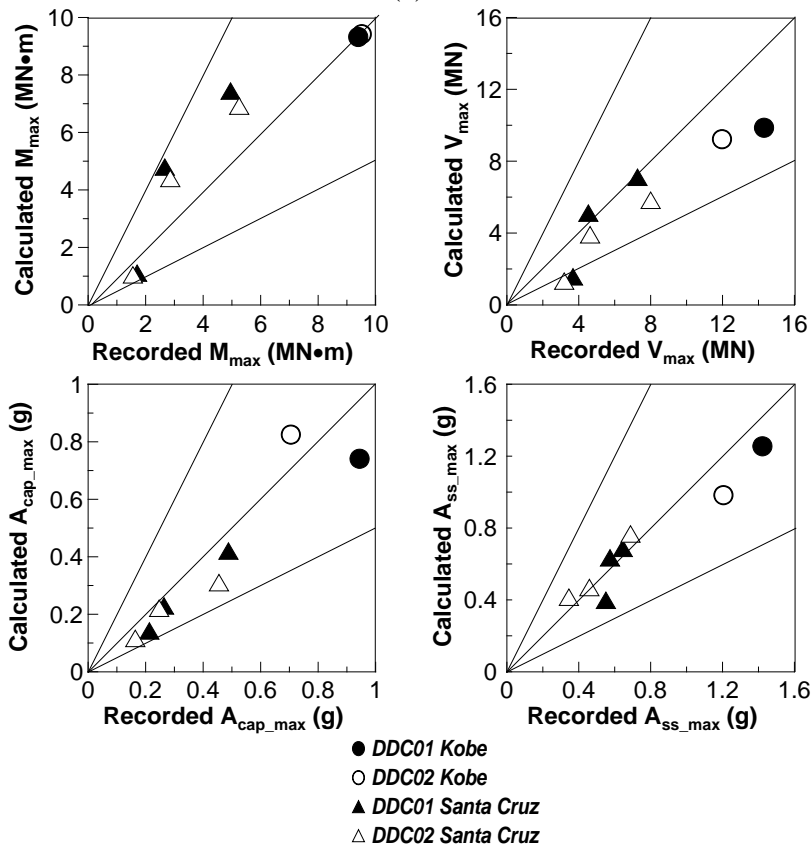


DDC01 in All Four Motions

Figure 9. Comparison of between recorded and computed total shear loads on the pile cap during big cycles of the four motions for centrifuge tests of the $T_{\text{fix_base}}=0.8$ s structure.



(a)



(b)

Figure 10. Comparison of between recorded and computed values for all 8 cases: (a) versus peak base acceleration, and (b) correlations between calculated and recorded values.

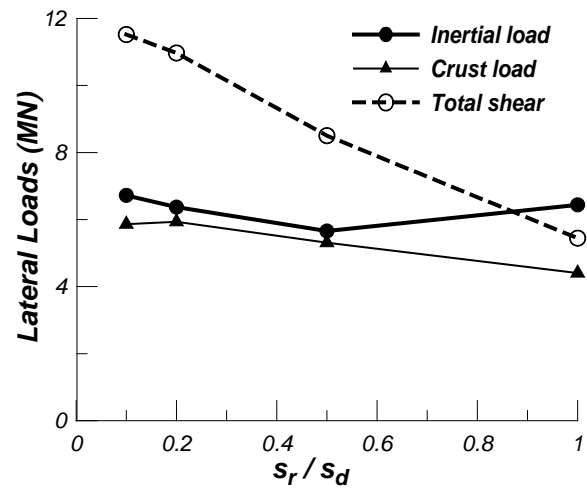


Figure 11. Sensitivity study – Influence of the interface element strength (p_u) for the $T_{\text{fixed-base}} = 0.8$ s structure in the large Kobe motion.